eLIFE elifesciences.org

RESEARCH ARTICLE

Figures and figure supplements

Microglial transglutaminase-2 drives myelination and myelin repair via GPR56/ADGRG1 in oligodendrocyte precursor cells

Stefanie Giera *et al*

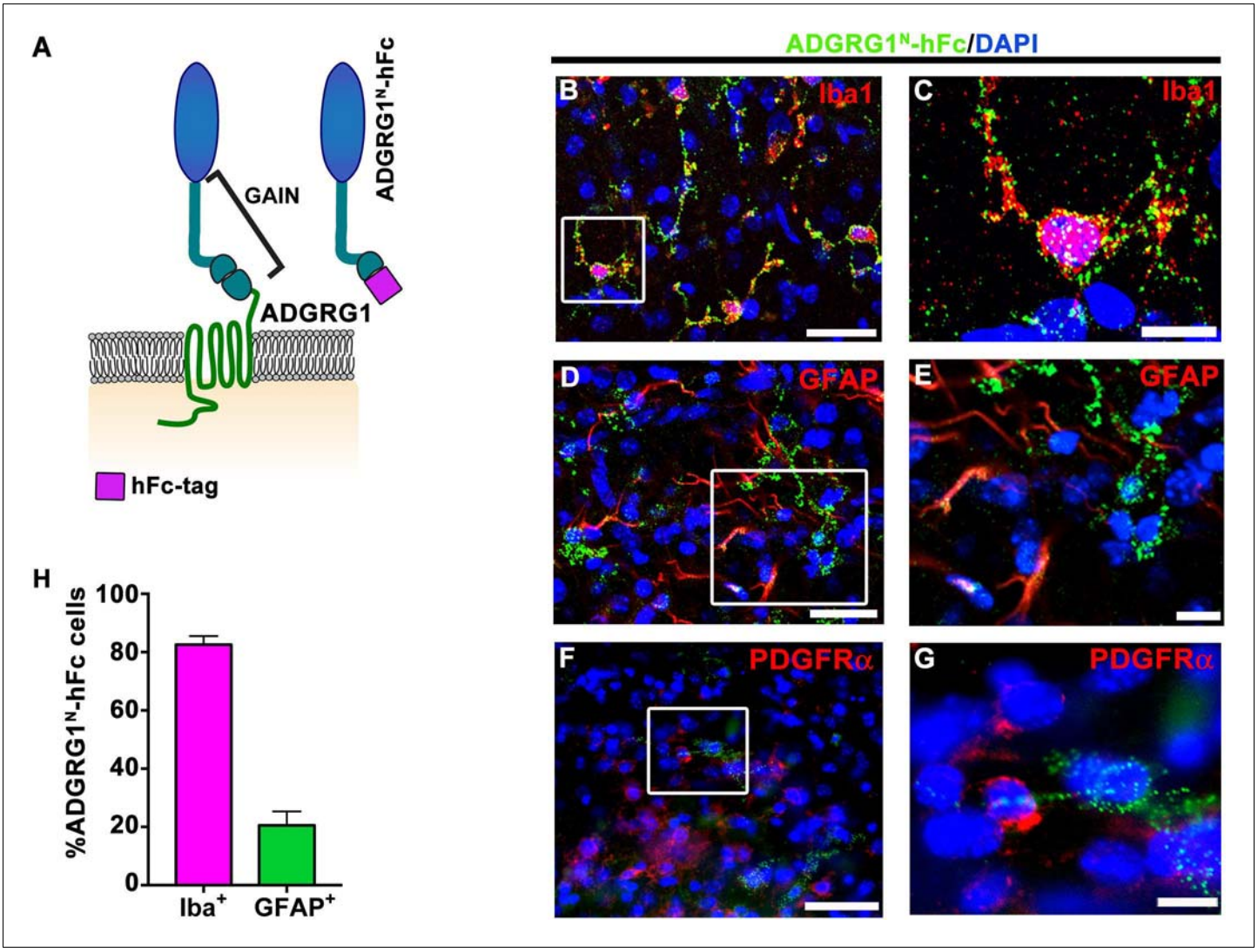

Figure 1. Microglia express the putative ligand of ADGRG1. (**A**) Schema of ADGRG1 receptor. GAIN domain and ADGRG1^{N}-hFc are shown. (**B, D,** and **F**) Double labeling of ADGRG1^{N}-hFc (green) and Iba1 (**B**, red), GFAP (**D**, red), PDGFRα (**F**, red) in P5 wt corpus callosum. DAPI, blue. Scale bar, 25 μm. (**C, E,** and **G**) Higher magnification of the boxed region in (**B, D** and **F**). Scale bar, 10 μm. Staining was repeated *N* = 3–4 animals. (**H**) Quantification of double positive ADGRG1^{N}-hFc^{+} and Iba^{+} cells and ADGRG1^{N}-hFc^{+} and GFAP^{+} cells. *N* = 3–4 per staining.

DOI: https://doi.org/10.7554/eLife.33385.002

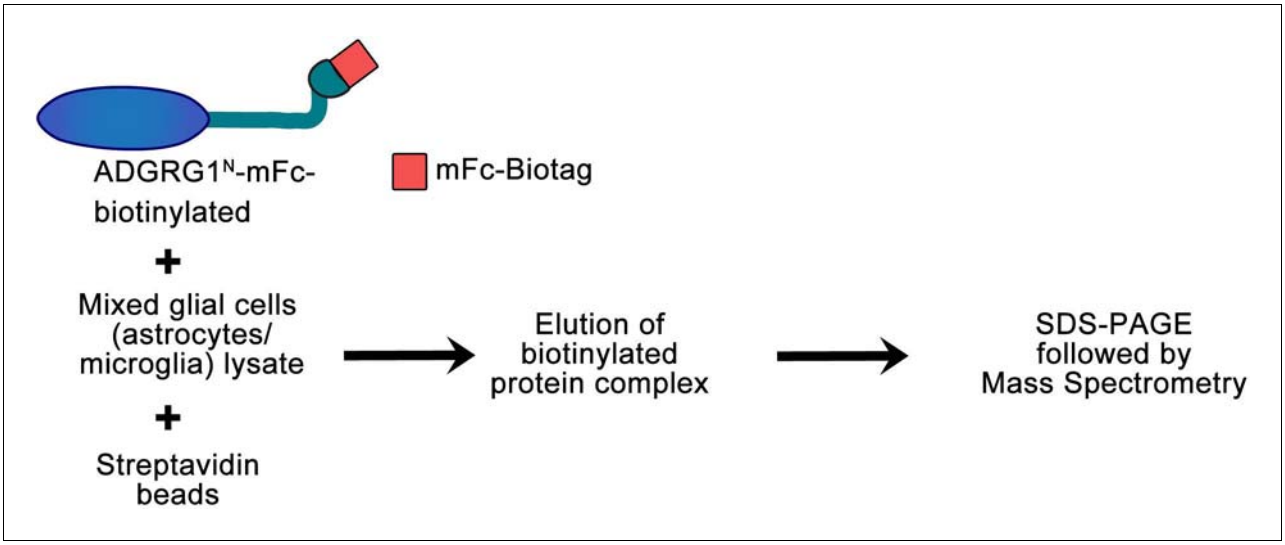

Figure 1—figure supplement 1. Flow chart of the in vitro biotinylation/proteomic approach. Biotinylated ADGRG1^{N}-mFc was used to purify ADGRG1 binding partner(s) from mixed glial cell (enriched in microglia and astrocytes) lysate. Protein complexes were subjected to SDS PAGE and tryptic peptide mass spectrometry protein identification after one-step purification with immobilized streptavidin. The whole lane was excised and subjected to tryptic peptide mass spectrometry (MS) protein identification analysis.

DOI: https://doi.org/10.7554/eLife.33385.003

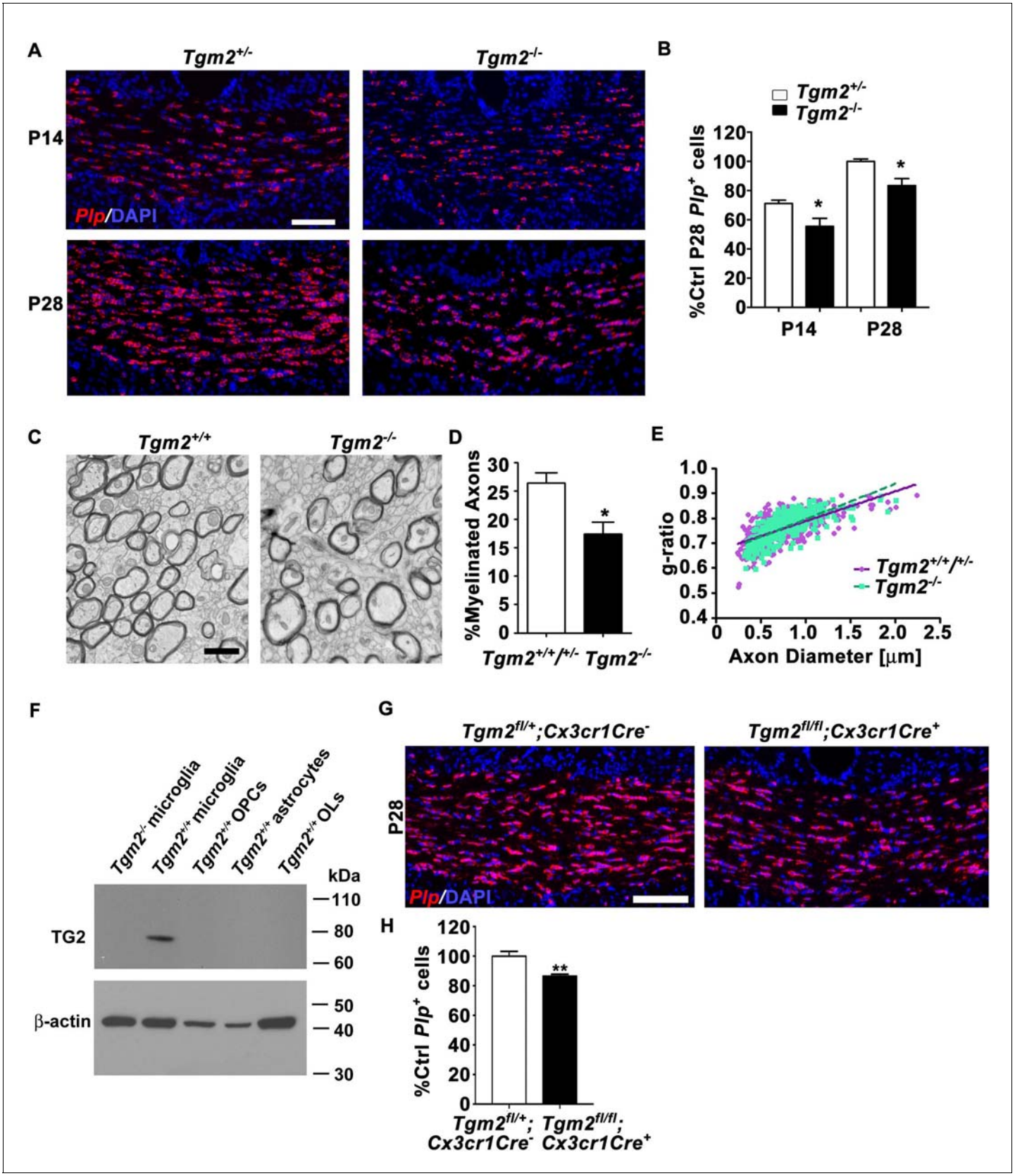

Figure 2. Loss of *Tgm2* leads to fewer mature OLs and hypomyelination in the CC. (**A**) Representative in situ hybridization (ISH) images of *Plp* (red) in the CC of P14 (top panel) and P28 (bottom panel) $Tgm2^{+/-}$ and $Tgm2^{-/-}$ mice. DAPI, blue. Scale bar, 100 μm. (**B**) Quantification of Plp^{+} oligodendrocytes

Figure 2 continued on next page

Figure 2 continued

from the CC of *Tgm2*$^{+/-}$ and *Tgm2*$^{-/-}$ P14 and P28 mice. * P=0.0484; *N* = 5 per genotype (**P14**); *p=0.0378; *N* = 4 per genotype (**P28**), unpaired *t*-test. (**C**) Representative TEM images from P28 CC of *Tgm2*$^{+/+}$ and *Tgm2*$^{-/-}$ mice. Scale bar, 1 μm. (**D**) Percentage of myelinated axons in the CC of control (*Tgm2*$^{+/+}$ and *Tgm2*$^{+/-}$) and *Tgm2*$^{-/-}$ mice. *p=0.0299; *N* = 3 per genotype; unpaired *t*-test. (**E**) Scatter plot displaying g-ratio values in the CC of control and *Tgm2*$^{-/-}$ mice. (**F**) TG2 western blot on acutely isolated microglia, OPCs, astrocytes, and mature oligodendrocytes from the P7 neonatal brain. *β*-actin was used as loading control. (**G**) Representative ISH images of *Plp* (red) in the CC of P28 *Tgm2*$^{fl/+}$;*Cx3cr1Cre*$^{-}$ and *Tgm2*$^{fl/fl}$;*Cx3cr1Cre* $^{+}$ mice. DAPI, blue. Scale bar, 100 μm. (**H**) Quantification of *Plp*$^{+}$ oligodendrocytes in the CC of P28 *Tgm2*$^{fl/+}$;*Cx3cr1Cre*$^{-}$ and *Tgm2*$^{fl/fl}$;*Cx3cr1Cre* $^{+}$ mice. **p=0.00850; *N* = 4 per genotype, unpaired *t*-test. Error bars are means ± s.e.m (**B, D, H**).

DOI: https://doi.org/10.7554/eLife.33385.005

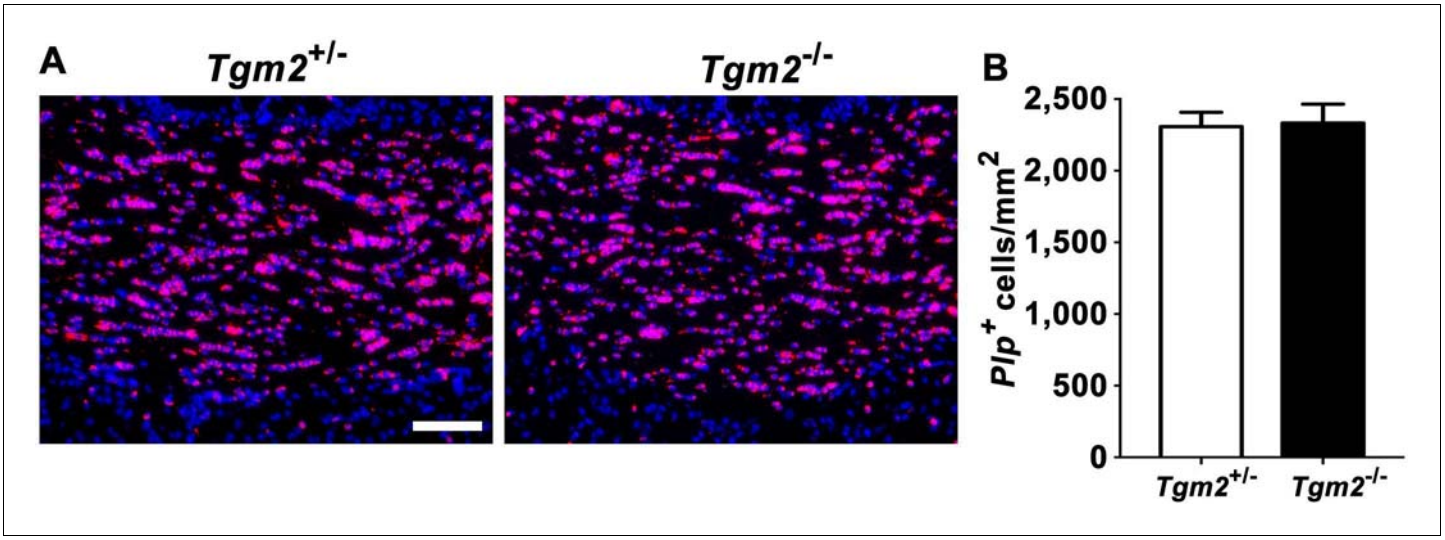

Figure 2—figure supplement 1. Oligodendrocyte number recovers by 5 month in *Tgm2* knockout mice. (**A**) Representative images of ISH of *Plp* in the CC of 4–5 month old $Tgm2^{+/-}$ and $Tgm2^{-/-}$ mice. Scale bar, 100 μm. DAPI, blue. (**B**) Quantification of Plp^{+} oligodendrocytes in the CC reveals similar numbers of OLs in the CC of $Tgm2^{+/-}$ and $Tgm2^{-/-}$ mice. * P=0.807, unpaired t-test, *N* = 3 per genotype. Error bars are means ± s.e.m.

DOI: https://doi.org/10.7554/eLife.33385.006

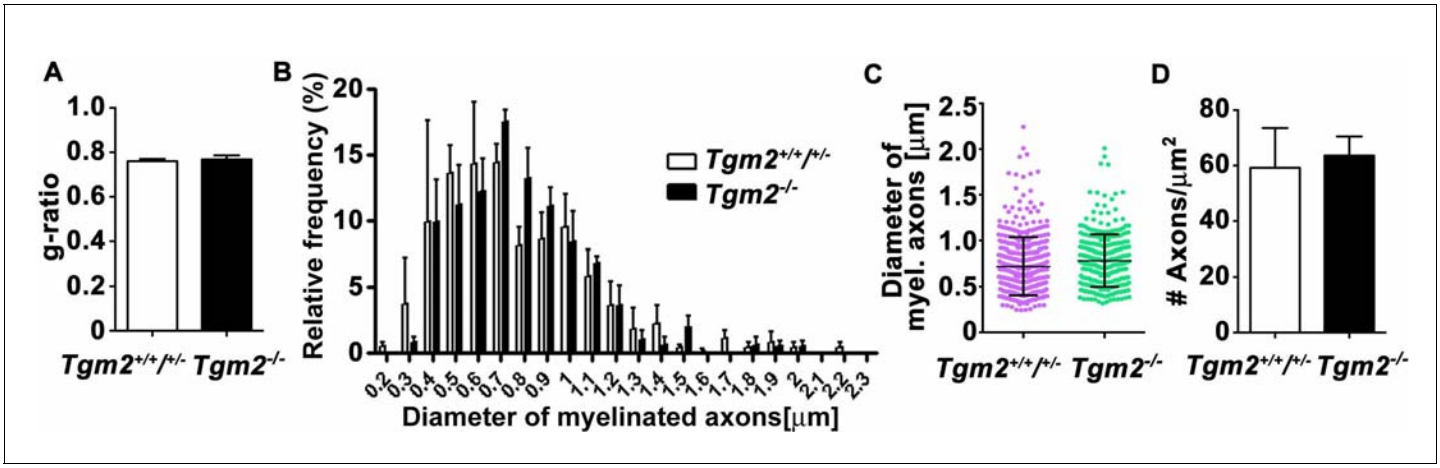

Figure 2—figure supplement 2. Loss of *Tgm2* does not affect g-ratio, myelinated axon distribution, axon diameter or axon number. (**A**) Average g-ratio of myelin sheath thickness was comparable in control and *Tgm2*$^{-/-}$ mice. p=0.728, unpaired t-test, *N* = 3 per genotype. (**B**) The distribution of myelinated axons with respect to the axon diameter in the CC of control and *Tgm2*$^{-/-}$ mice. p=0.8291, two-way ANOVA, p=0.2524, Gaussian non-linear curve fit, *N* = 3 per genotype. (**C**) Axon diameter in the CC is comparable in control and *Tgm2*$^{-/-}$ mice. Mean ± s.d.; p=0.8771; unpaired *t*-test; *N* = 3 per genotype. (**D**) Number of total axons (myelinated and unmyelinated) is comparable in the CC of in control and *Tgm2*$^{-/-}$ mice at P28. p=0.7947, unpaired *t*-test, *N* = 3 per genotype. Error bars are means ± s.e.m (**A–D**).

DOI: https://doi.org/10.7554/eLife.33385.007

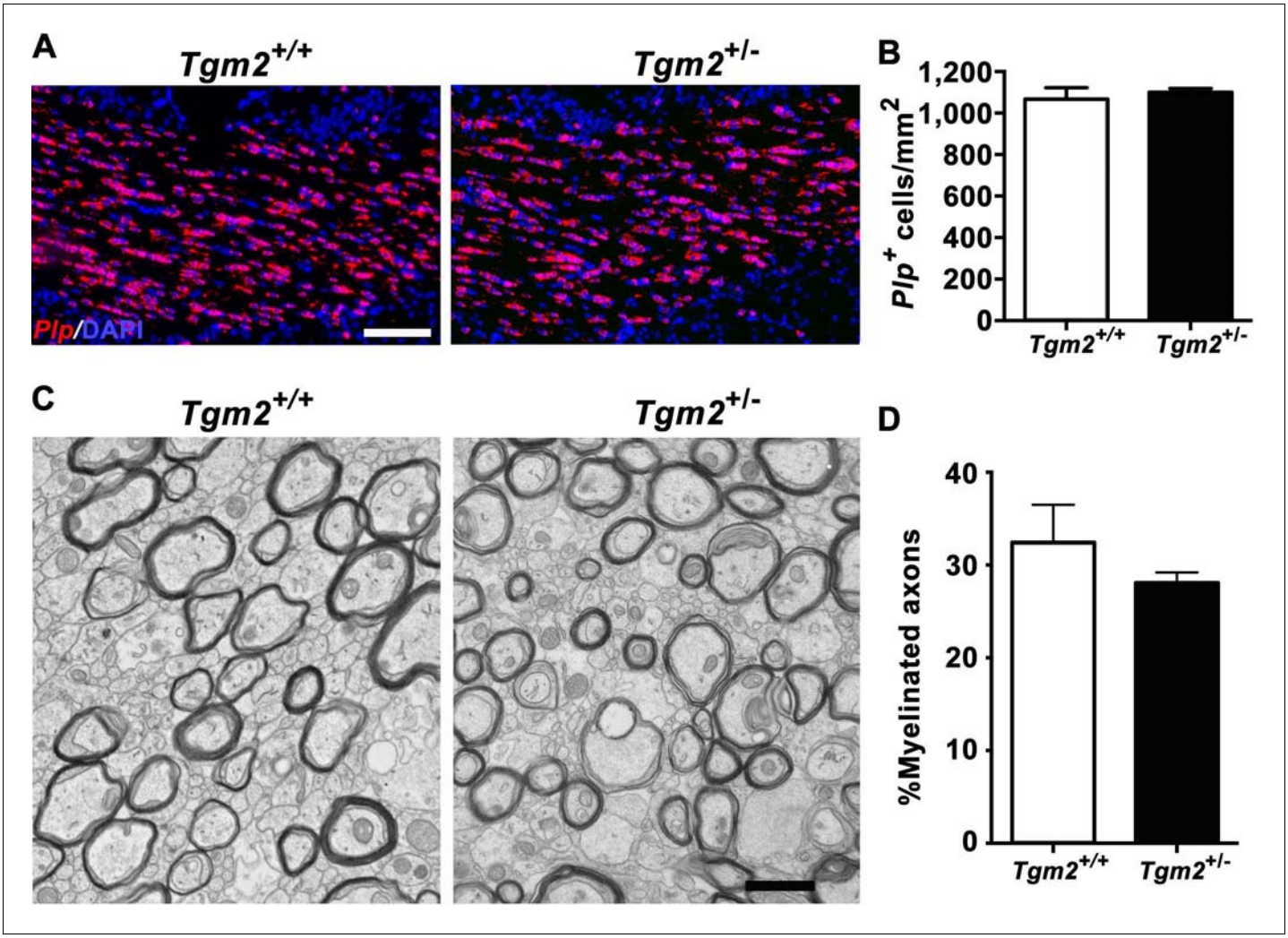

Figure 2—figure supplement 3. Deleting one allele of *Tgm2* has no effect on the number of Plp^+ + and myelinated axons. (**A**) Representative images of ISH of *Plp* on P28 in the CC in $Tgm2^{+/+}$ and $Tgm2^{+/-}$ 100 µm. Scale bar, 100 µm. DAPI, blue. (**B**) Quantification of Plp^+ oligodendrocytes in the CC reveals similar numbers of OLs in the CC of $Tgm2^{+/+}$ and $Tgm2^{+/-}$ mice. *p=0.6005, unpaired t-test, *N* = 3 per genotype. (**C**) Representative TEM images from P28 CC of $Tgm2^{+/+}$ and $Tgm2^{+/-}$ mice. Scale bar, 1 µm. (**D**) Percentage of myelinated axons was quantified in the CC in $Tgm2^{+/+}$ and $Tgm2^{+/-}$ mice. p=0.5129, unpaired t-test, *N* = 3 per genotype. Error bars are means ± s.e.m (**B, D**).

DOI: https://doi.org/10.7554/eLife.33385.008

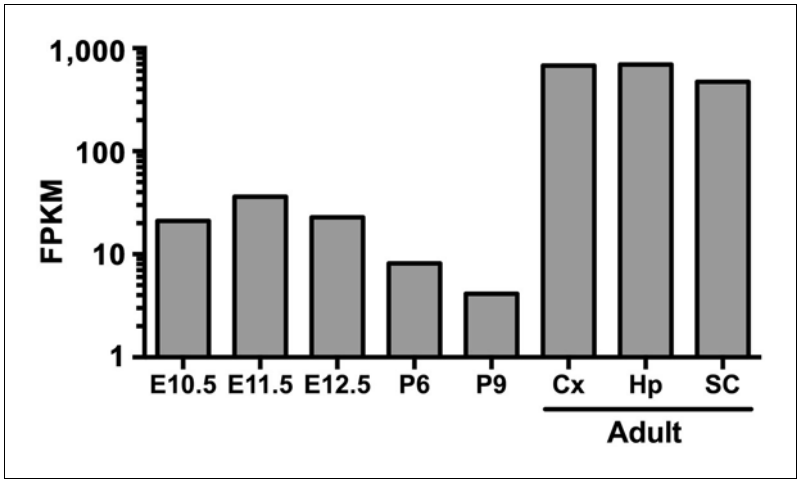

Figure 2—figure supplement 4. Developmental expression of *Tgm2*. Developmental expression of *Tgm2* in murine microglia purified from whole brains (E10.5 through P) or brain regions (adult) at the indicated embryonic and postnatal ages. RNA-sequencing data was extracted from public database of (***Matcovitch-Natan et al., 2016***). Cx: cortex, Hp: hippocampus, SC: spinal cord.

DOI: https://doi.org/10.7554/eLife.33385.009

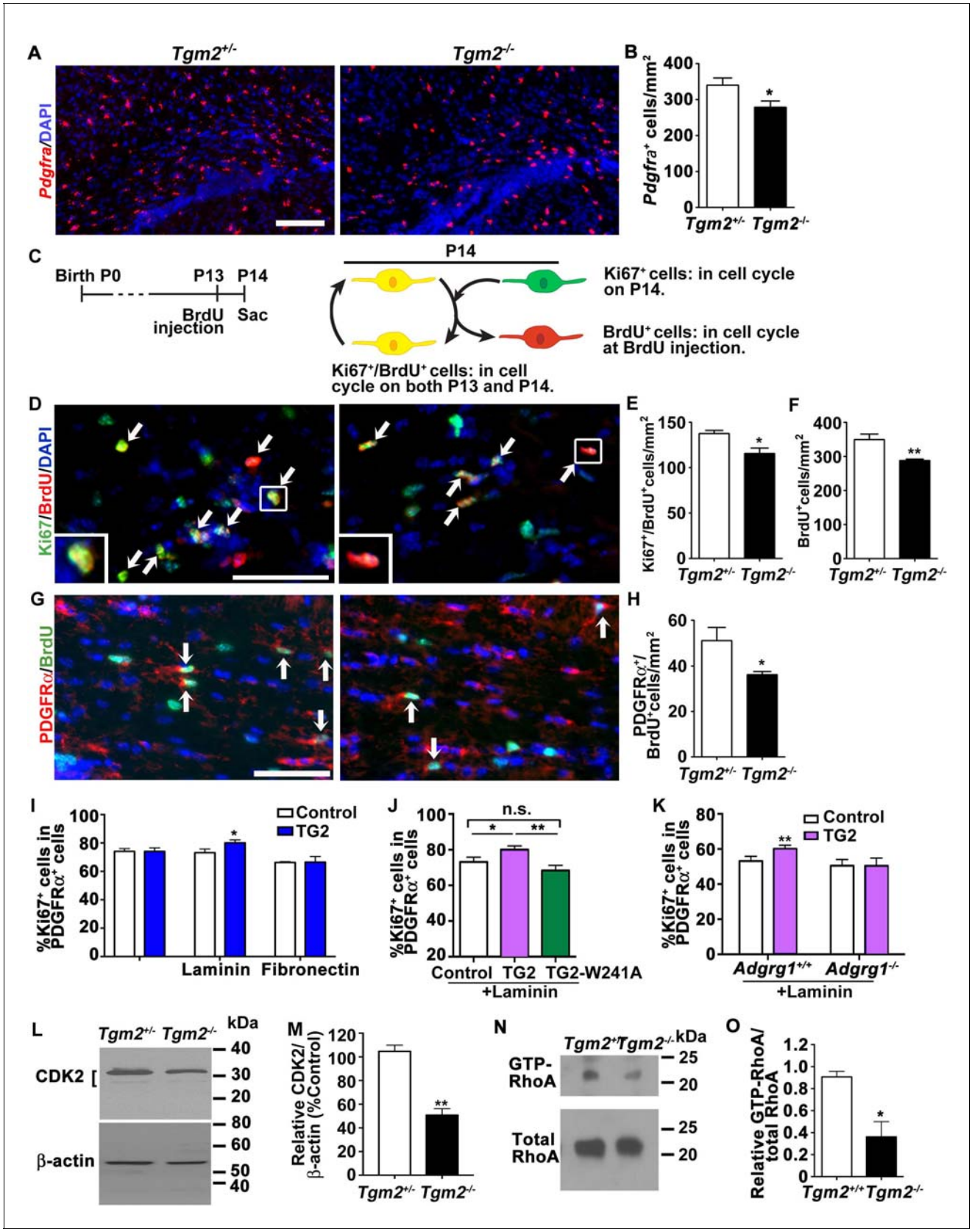

Figure 3. TG2 regulates OPC proliferation through ADGRG1. (**A**) Representative ISH images of *Pdgfra* (red) in the CC of P14 *Tgm2*$^{+/-}$ and *Tgm2*$^{-/-}$ mice. DAPI, blue. Scale bar, 100 μm. (**B**) Quantification of *Pdgfra*$^{+}$ OPCs in the CC of control and *Tgm2*$^{-/-}$ mice. *p=0.0320, unpaired t-test, *N* = 6 per

Figure 3 continued on next page

Figure 3 continued

genotype. (**C**) Cartoon showing the cell cycle exit assay. (**D**) Representative images of double IHC of BrdU (red) and Ki67 (green) in the CC of P14 *Tgm2*$^{+/-}$ and *Tgm2*$^{-/-}$ mice that were pulsed with BrdU 24 hr earlier (arrows mark double positive Ki67^{+}/BrdU^{+} cells). DAPI, blue. Scale bar, 50 μm. (**E**) The density of Ki67^{+}/BrdU^{+} cells in the CC is lower in *Tgm2*$^{-/-}$ mice. *p=0.0207, unpaired *t*-test, *N* = 5 per genotype. (**F**) The density of BrdU^{+} cells in the CC is reduced in *Tgm2*$^{-/-}$ mice. **p=0.0099, unpaired *t*-test, *N* = 5 per genotype. (**G**) Representative images of double IHC of PDGFRα (red) and BrdU (green) in the CC of P14 *Tgm2*$^{+/-}$ and *Tgm2*$^{-/-}$ mice (arrows mark double positive PDGFRα^{+}/BrdU^{+}cells). DAPI, blue. Scale bar, 50 μm. (**H**) The number of BrdU^{+}/PDGFRα^{+} cells in the CC is reduced in *Tgm2*$^{-/-}$ mice. *p=0.0465, unpaired *t*-test, *N* = 4 per genotype. Error bars are means ± s.e.m. (**I**) The effect of recombinant TG2 (rTG2) on OPC proliferation in basal condition, laminin-111 or fibronectin. rTG2 stimulates OPC proliferation only in the presence of laminin-111. *p=0.039, paired t-test, *N* = 3–6 per group. (**J**) The effect of wild type TG2 and its enzymatic dead mutant TG2-W241A proteins on OPC proliferation. Only wild type TG2 stimulates OPC proliferation. **p=0.0091; One-way ANOVA followed by Tukey post-hoc test, F(2,14) = 6.7, *p=0.05 (control vs. rTG2); n.s. p=0.70 (control vs. TG2-W241A); **p=0.0088 (TG2 vs. TG2-W241A); (**K**) *Adgrg1*$^{-/-}$ OPCs fail to respond to rTG2-enhanced proliferation. *p=0.0063, paired t-test, *N* = 5 per genotype. (**L**) Western blot analyses of CDK2 in acutely isolated OPCs from P7 *Tgm2*$^{+/-}$ and *Tgm2*$^{-/-}$ brains. The bracket indicates CDK2 protein isoform bands. β-actin was used as loading control. (**M**) CDK2 protein levels are reduced in the *Tgm2*$^{-/-}$ mice. ±=0.002, unpaired t-test, *N* = 3 per genotype. (**N**) Western blot of active RhoA (top panel) and total RhoA (bottom panel) in the CC of *Tgm2*$^{+/+}$ and *Tgm2*$^{-/-}$ mice. (**O**) The relative level of active RhoA to total RhoA was diminished in the CC of *Tgm2*$^{-/-}$ mice compared to *Tgm2*$^{+/+}$ control mice. *p=0.0207, unpaired *t*-test, *N* = 3 per genotype. Error bars are means ± s.e.m (**B, E, F, H, I, J, K, M, O**).

DOI: https://doi.org/10.7554/eLife.33385.010

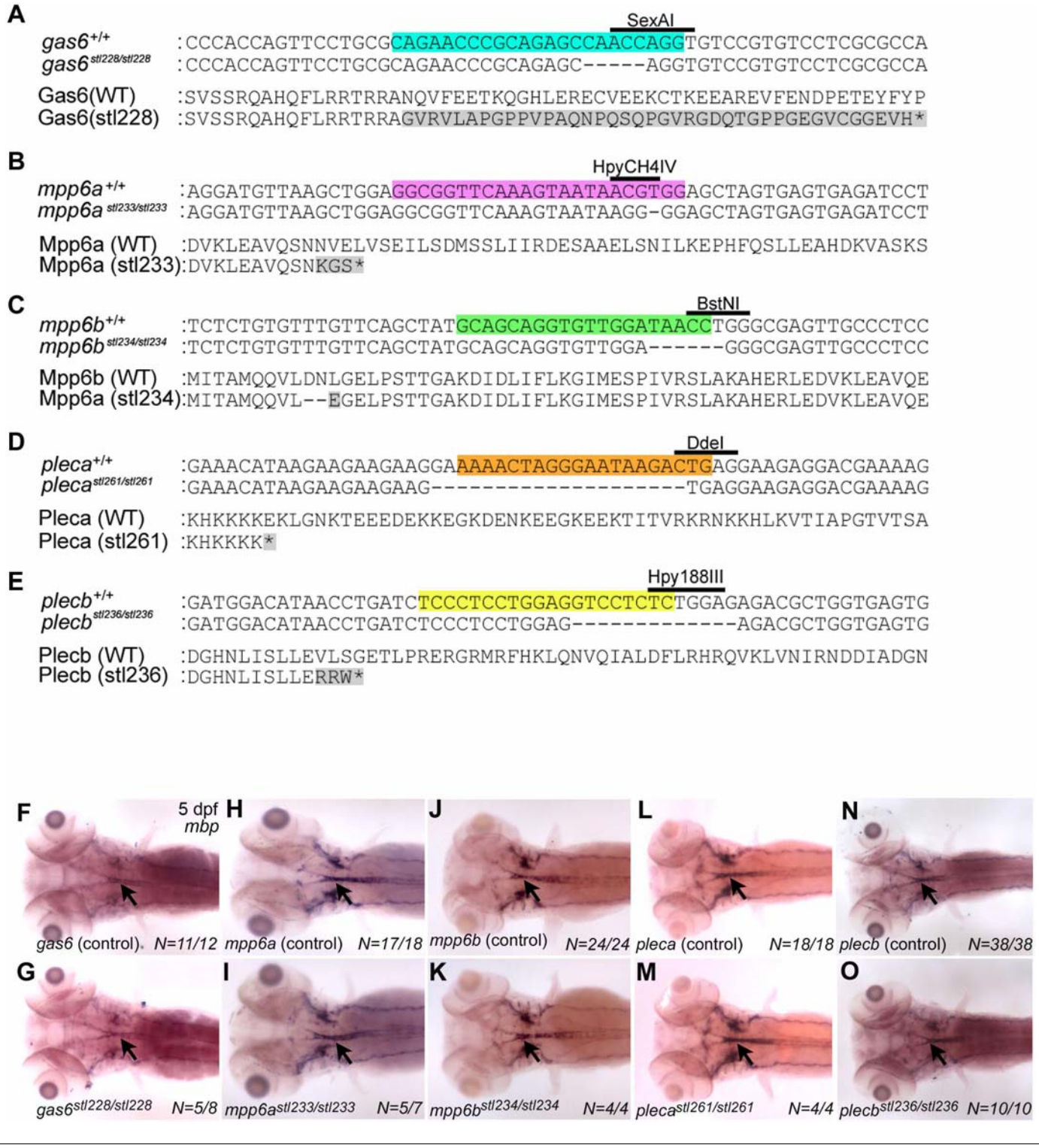

Figure 3—figure supplement 1. Mutations in *gas6*, *mpp6*, and *plec* do not affect CNS Mbp expression. (**A–E**) CRISPR-Cas9 technology was used to generate mutations in zebrafish *gas6* (**A**), *mpp6a* (**B**), *mpp6b* (**C**), *pleca* (**D**), and *plecb* (**E**). (**A**) A CRISPR/Cas9 system guide RNA (gRNA) designed to disrupt exon 2 (targeted sequence highlighted blue and SexAI restriction enzyme site used for genotyping denoted) of *gas6* generated *gas6*^{stl228}, a 4 bp deletion predicted to result in a frameshift and premature STOP. Alignments of wt and mutant nucleotide sequences (top), and predicted wt (706 aa) and mutant (78 aa) protein sequences (bottom) shown. (**B**) A gRNA designed to disrupt the 3rd coding exon 5 (targeted sequence highlighted

Figure 3—figure supplement 1 continued on next page

Figure 3—figure supplement 1 continued

purple, and HpyCH4IV restriction enzyme site used for genotyping denoted) of *mpp6a* generated *mpp6a*^{stl233}, a 1 bp deletion predicted to result in a frameshift and premature STOP. Alignments of wt and mutant nucleotide sequences (top), and predicted wt (550 aa) and mutant (69 aa) protein sequences (bottom) shown. (**C**) A gRNA designed to disrupt exon 2 (targeted sequence highlighted green and BstNI restriction enzyme site used for genotyping denoted) of *mpp6b* generated *mpp6b*^{stl234}, a 6 bp deletion predicted to result in a two amino acid deletion and a single amino acid change within the receptor targeting domain. Alignments of wt and mutant nucleotide sequences (top), and predicted wt (539 aa) and mutant (537 aa) protein sequences (bottom) shown. (**D**) A gRNA designed to disrupt exon 3 (targeted sequence highlighted orange, and DdeI restriction enzyme site used for genotyping denoted) of *pleca* generated *pleca*^{stl261}, a 20 bp deletion predicted to result in a frameshift and premature STOP. Alignments of wt and mutant nucleotide sequences (top), and predicted wt (4752 aa) and mutant (103 aa) protein sequences (bottom) shown. (**E**) A gRNA designed to disrupt the 3rd coding exon (targeted sequence highlighted yellow, and Hpy188III restriction enzyme site used for genotyping denoted) of *plecb* generated *plecb*^{stl236}, a 13 bp deletion predicted to result in a frameshift and premature STOP. Alignments of wt and mutant nucleotide sequences (top), and predicted wt (4530 aa) and mutant (111 aa) protein sequences (bottom) shown. (**F– O**) Whole mount ISH showing *mbp* expression (CNS denoted by black arrows) at 5 days post-fertilization (dpf) in (**F**) *gas6* control larva (wt and *gas6*$^{stl228/+}$, *N = 11/12*), (**G**) *gas*$^{stl228/stl228}$ mutant larva (*N = 5/8*), (**H**) *mpp6a* control larva (wt and *mpp6a*$^{stl233/+}$, *N = 17/18*), (**I**) *mpp6a*$^{stl233/stl233}$ mutant larva (*N = 5/7*), (**J**) *mpp6b* control larva (wt and *mpp6b*$^{stl234/+}$, *N = 24/24*), (**K**) *mpp6b*$^{stl234/stl234}$ (*N = 4/4*), (**L**) *pleca* control larva (wt and *pleca*$^{stl261/+}$, *N = 18/18*), (**M**) *pleca*$^{stl261/stl261}$mutant larva (*N = 4/4*), (**N**) *plecb* control larva (wt and *plecb*$^{stl236/+}$, *N = 36/38*), and (**O**) *plecb*$^{stl236/st'236}$ mutant larva (*N = 10/10*). Dorsal views are shown for all, anterior to the left. No gross changes in *mbp* expression were observed in putative ligand mutants relative to sibling controls.

DOI: https://doi.org/10.7554/eLife.33385.011

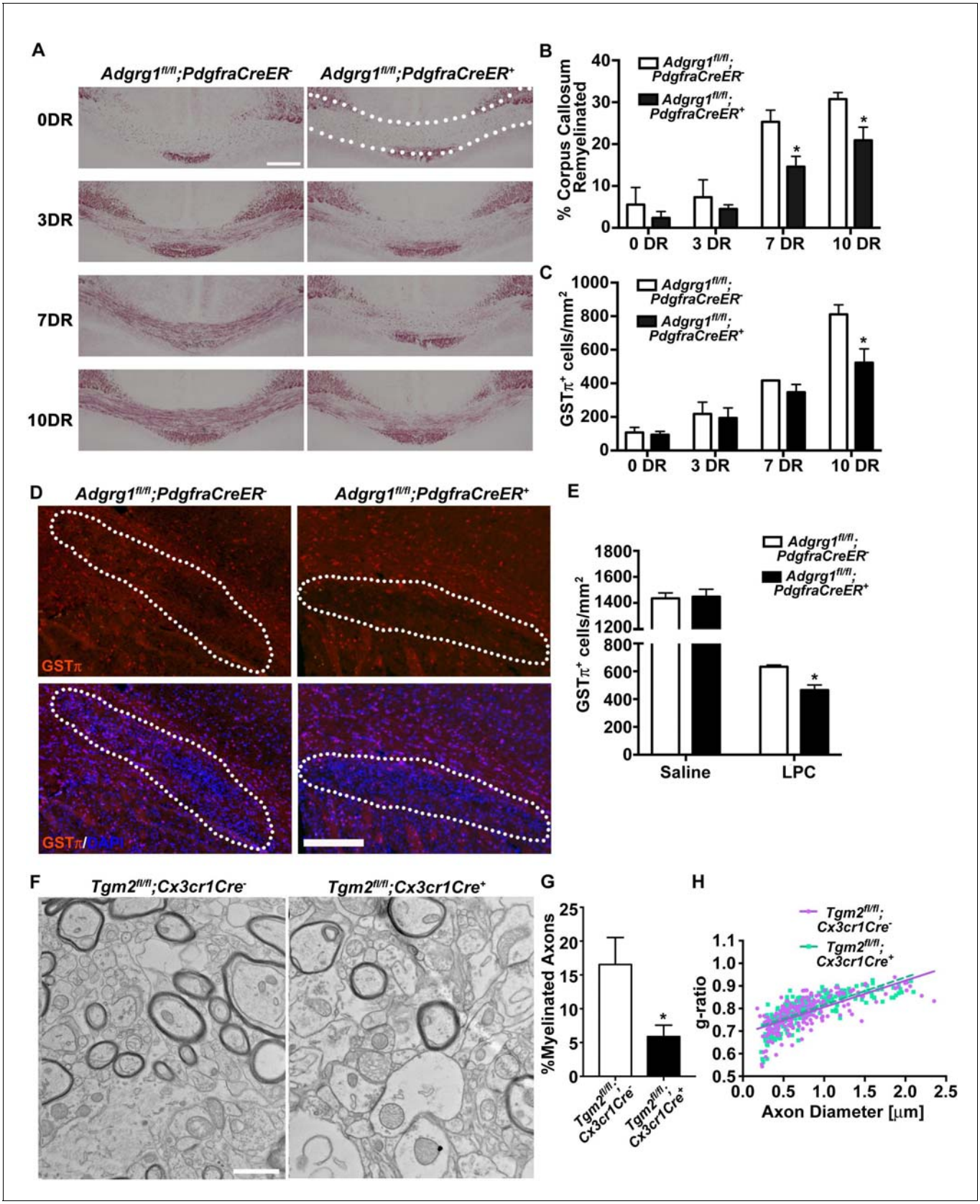

Figure 4. ADGRG1 is required for remyelination in vivo. (**A**) Representative images of Black-Gold myelin staining of the corpus callosum of *Adgrg1*$^{fl/fl}$;*PdgfraCreER*$^{-}$ and *Adgrg1*$^{fl/fl}$;*PdgfraCreER*$^{+}$ + after cuprizone feeding for 6 weeks followed by recovery for 3 d (3 DR), 7 d (7 DR) and 10 d (10 DR)

Figure 4 continued on next page

Figure 4 continued

(dotted line outlines quantified region). Scale bar, 250 μm. (**B**) Percentage of remyelinated corpus callosum displayed significant decrease in myelination at 7 DR and 10 DR between *Adgrg1$^{fl/fl}$;PdgfraCreER^{-}* and *Adgrg1$^{fl/fl}$;PdgfraCreER^{+}* +. *p=0.0285 (7 DR), *N = 4 (cre^{-}); N = 4 (cre^{+});* *p=0.0416 (10 DR), *N = 3 (cre^{-}); N = 4 (cre^{+}),* unpaired *t*-test. (**C**) Number of GSTπ^{+} OLs are significantly decreased at 10 DR between *Adgrg1$^{fl/fl}$;PdgfraCreER^{-}* and *Adgrg1$^{fl/fl}$;PdgfraCreER^{+}* +. *p=0.0457 (10 DR), *N = 3 (cre^{-}); N = 3 (cre^{+}),* unpaired *t*-test. (**D**) Representative images of GSTπ^{+} OLs in the corpus callosum of *Adgrg1$^{fl/fl}$;PdgfraCreER^{-}* and *Adgrg1$^{fl/fl}$;PdgfraCreER^{+}* + 14 days post-lesion (dotted line outlines quantified region). Scale bar, 200 μm. (**E**) Number of GSTπ^{+} OLs are significantly decreased 14 days post-lesion between *Adgrg1$^{fl/fl}$;PdgfraCreER^{-}* and *Adgrg1$^{fl/fl}$;PdgfraCreER^{+}* +. *p=0.0133, *N = 3 (cre^{-}); N = 3 (cre^{+}),* unpaired *t*-test. (**F**) Representative TEM images from the CC of *Tgm2$^{fl/fl}$;Cx3cr1Cre^{-}* and *Tgm2$^{fl/fl}$;Cx3cr1Cre^{+}* mice. Scale bar, 1 μm. (**D**) Percentage of myelinated axons in the CC of *Tgm2$^{fl/fl}$;Cx3cr1Cre^{-}* and *Tgm2$^{fl/fl}$;Cx3cr1Cre^{+}* mice. *p=0.0493; *N* = 4 per genotype; unpaired *t*-test. (**E**) Scatter plot displaying g-ratio values in the CC of *Tgm2$^{fl/fl}$;Cx3cr1Cre^{-}* and *Tgm2$^{fl/fl}$;Cx3cr1Cre^{+}* mice.

DOI: https://doi.org/10.7554/eLife.33385.012

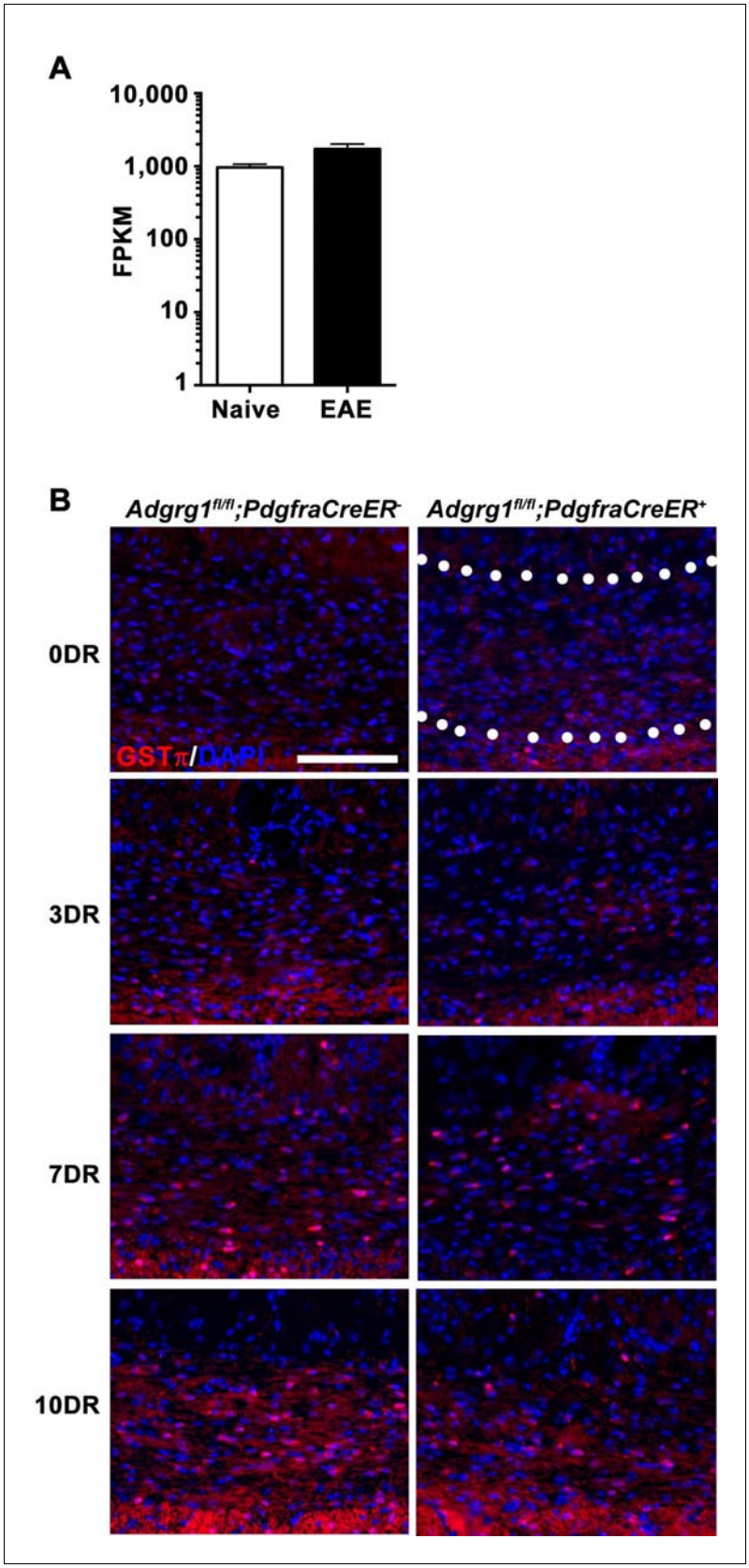

Figure 4—figure supplement 1. Loss of *Adgrg1* in the OL lineage leads to reduced numbers of myelinating OLs. (**A**) Expression of *Tgm2* in murine microglia purified from naive or EAE brains. RNA-sequencing data was extracted

Figure 4—figure supplement 1 continued on next page

Figure 4—figure supplement 1 continued

from public database of (***Wlodarczyk et al., 2017***). (**B**) Representative images of GSTπ^{+} OLs of the corpus callosum of *Adgrg1$^{fl/fl}$;PdgfraCreER^{-}* and *Adgrg1$^{fl/fl}$;PdgfraCreER^{+}* mice after cuprizone feeding for 6 weeks followed by recovery for 3 d (3 DR), 7 d (7 DR) and 10 d (10 DR) (dotted line outlines quantified region). Scale bar, 100 μm.

DOI: https://doi.org/10.7554/eLife.33385.013

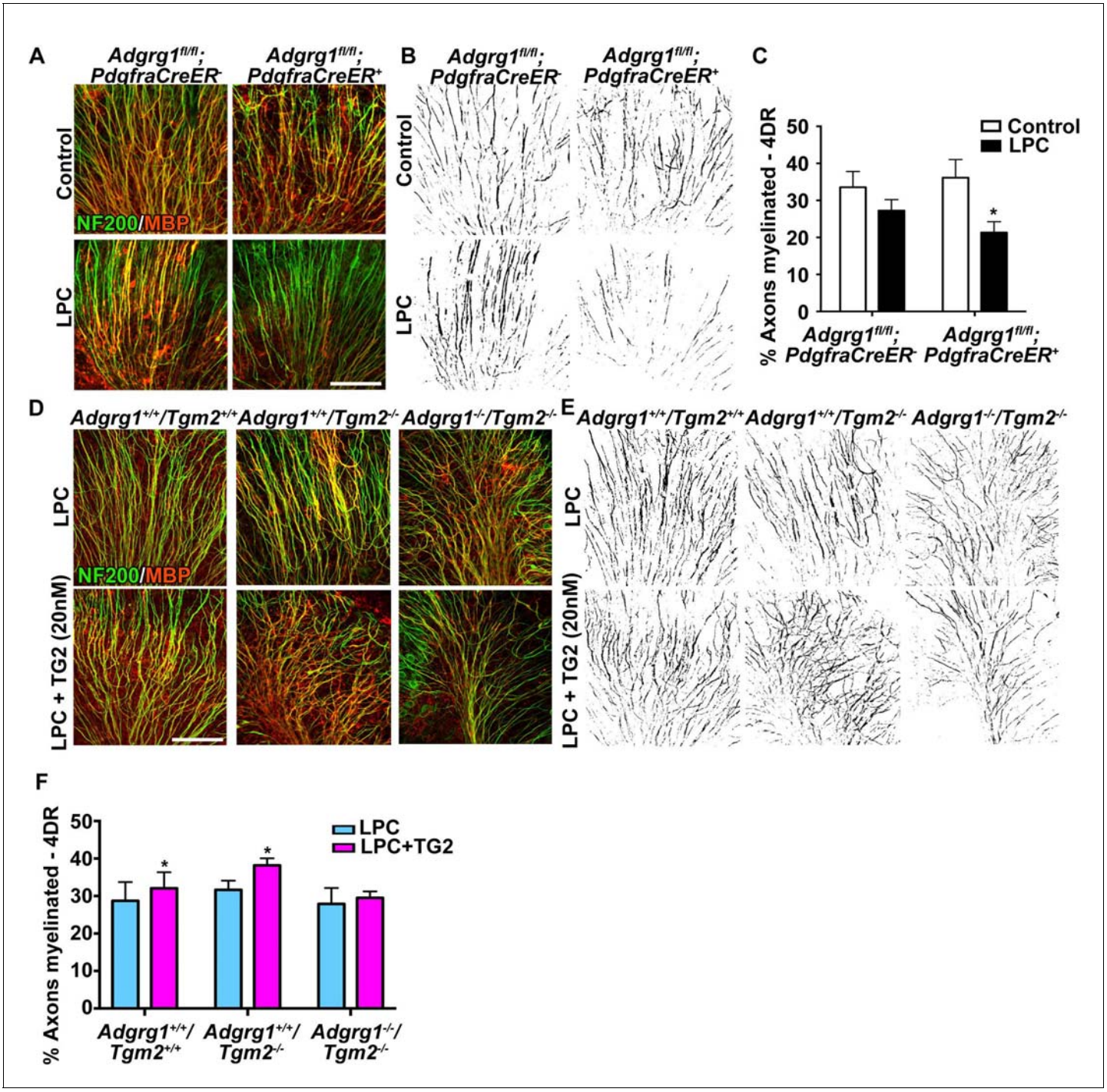

Figure 5. ADGRG1 and its ligand TG2 are required for remyelination. (**A**) Representative images of cerebellar slice cultures from P10 *Adgrg1$^{fl/fl}$; PdgfraCreER^{-}* and *Adgrg1$^{fl/fl}$;PdgfraCreER^{+}* + cerebella that were demyelinated with LPC for 24 hr followed by 4 days of recovery (4DR). Slices were labeled with NF200 (green) and MBP (red); myelinated fibers appear yellow in merged images. Scale bar, 100 μm. (**B**) Composite images created in Image J show myelinated axons (black) for quantification. (**C**) Percentage of myelinated axons after remyelination. Remyelination is reduced in cerebellar slices that lack OPC-derived ADGRG1. *p=0.0135, paired *t*-test, *N* = 5 per genotype. (**D**) Representative images of cerebellar slice cultures from P10 *Adgrg1$^{+/+}$;Tgm2$^{+/+}$*, *Adgrg1$^{+/+}$;Tgm2$^{-/-}$* and *Adgrg1$^{-/-}$;Tgm2$^{-/-}$* mouse cerebella that were demyelinated with LPC for 24 hr followed by 4 days of remyelination in the presence or absence of rTG2 (20 nM). Slices were immunostained with NF200 (green) and MBP (red); myelinated fibers appear yellow in merged images. Scale bar, 100 μm. (**E**) Composite images created in Image J show myelinated axons (black) for quantification. (**F**) Percentage of myelinated axons. Recombinant TG2 promotes remyelination in *Adgrg1$^{+/+}$;Tgm2$^{+/+}$ and Adgrg1$^{+/+}$;Tgm2$^{-/-}$*, but not *Adgrg1$^{-/-}$;Tgm2$^{-/-}$* cerebellar slices. *p=0.0475 (*Adgrg1$^{+/+}$;Tgm2$^{+/+}$*), *p=0.0197 (*Adgrg1$^{+/+}$;Tgm2$^{-/-}$*), paired *t*-test, *N* = 5–6 per genotype. Error bars are mean ± s.e.m (**C, F**)..

DOI: https://doi.org/10.7554/eLife.33385.014

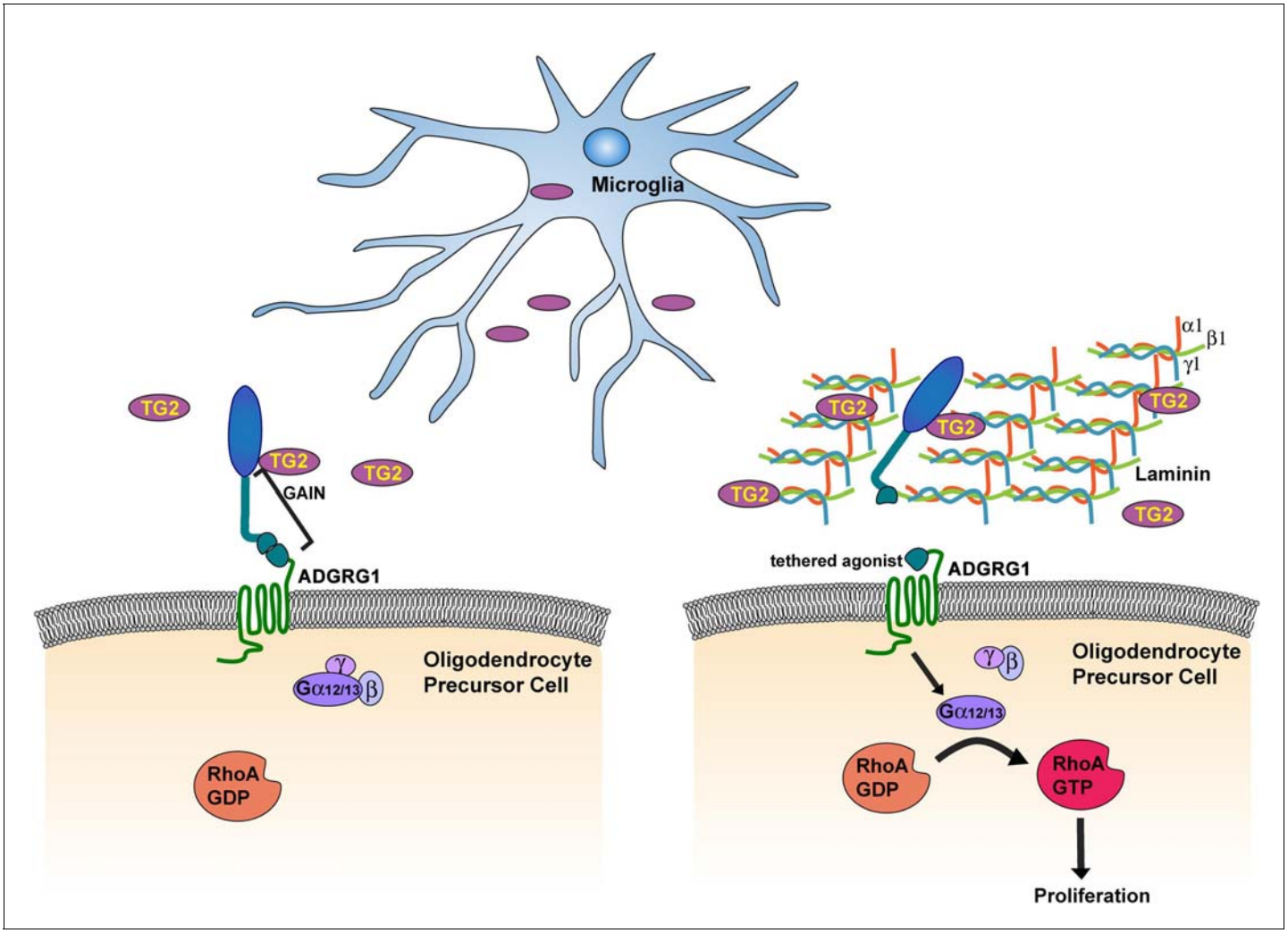

Figure 6. Microglia promote OPC proliferation via ADGRG1 signaling. TG2, secreted by microglia, binds ADGRG1 but fails to activate the receptor in the absence of ECM protein laminin-111. The binding of TG2 and laminin-111 to ADGRG1 leads to the dissociation of the ADGRG1 NTF from its CTF, allowing the tethered agonist to initiate G-protein signaling, culminating in activated RhoA, which promotes OPC proliferation. GAIN, GPCR-Autoproteolysis-INducing.

DOI: https://doi.org/10.7554/eLife.33385.015